Physics Letters A 176 (1993) 118–129
North-Holland

PHYSICS LETTERS A

Calorimetry of the Pd–D_2O system: from simplicity via complications to simplicity

Martin Fleischmann
Department of Chemistry, University of Southampton, Southampton, UK

and

Stanley Pons
IMRA EUROPE, Sophia Antipolis, 06560 Valbonne, France

Received 21 December 1992; revised manuscript received 4 March 1993; accepted for publication 8 March 1993
Communicated by J.P. Vigier

We present here one aspect of our recent research on the calorimetry of the Pd–D_2O system which has been concerned with high rates of specific excess enthalpy generation (> 1 kW cm^{-3}) at temperatures close to (or at) the boiling point of the electrolyte solution. This has led to a particularly simple method of deriving the rate of excess enthalpy production based on measuring the times required to boil the cells to dryness, this process being followed by using time-lapse video recordings. Our use of this simple method as well as our investigations of the results of other research groups prompts us to present also other simple methods of data analysis which we have used in the preliminary evaluations of these systems.

1. Introduction

One of our major objectives in developing the calorimetry of Pd and Pd-alloy cathodes polarised in D_2O solutions [1–7] has been to find simple illustrations of the fact that there is excess enthalpy generation in these electrodes whereas there is no such effect for Pd-based cathodes polarised in H_2O (nor for that matter, for Pt cathodes polarised in D_2O solutions). The simplest illustrations are purely qualitative: we have already drawn attention to the fact that, after prolonged polarisation, one can sometimes observe regions in which there is an increase of temperature accompanied by a decrease of cell potential with time for Pd-based cathodes such as that shown in fig. 1. The design of the Dewar-type calorimeters used in these experiments is illustrated in fig. 2. In the versions in current use the silvering of the top portion ensures that the heat transfer is controlled by radiation across the lower unsilvered part. The heat transfer coefficient controlling heat transfer to the surrounding water bath is then nearly independent of time provided the level of the electrolyte remains in the upper, silvered, zone. One can therefore pose the question: "How can it be that the temperature of the cell contents increases whereas the enthalpy input decreases with time?" Our answer to this dilemma naturally has been: "There is a source of enthalpy in the cells whose strength increases with time." At a more quantitative level one sees that the magnitudes of these sources are such that explanations in terms of chemical changes must be excluded [7].

Indeed, information of this kind was already included in our first major publication [1]. As the Dewar calorimeters used in that study were not silvered in the top region, the heat transfer coefficients decreased with time following each refilling of the cells (to make up for losses of D_2O due to electrolysis and evaporation). The purely qualitative conclusion "there is a source of excess enthalpy in the cells" was therefore confined to

0375-9601/93/$ 06.00 © 1993 Elsevier Science Publishers B.V. All rights reserved.

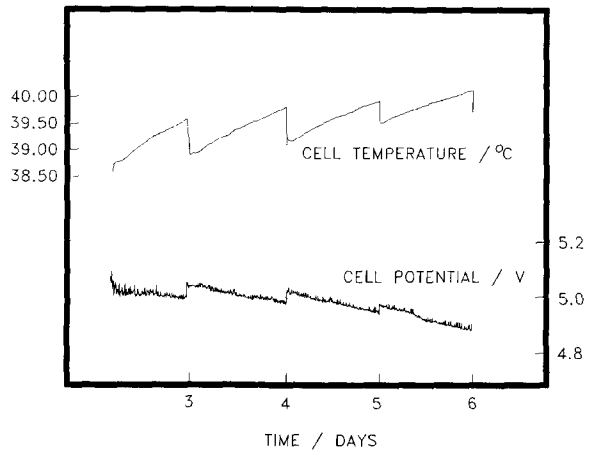

Fig. 1. Cell temperature (upper) and cell potential (lower) versus time since the cell was started for the electrolysis of D_2O in 0.6M Li_2SO_4 solution at pH 10 at a palladium rod cathode (0.4×1.25 cm). The cell current was 400 mA, the water bath temperature was 30.00°C, and the room temperature was 21°C. The rate of excess enthalpy generation at the end of each day was 0.045 W (day 3), 0.066 W (day 4), 0.086 W (day 5), and 0.115 W (day 6). The accumulation of excess enthalpy for this period was on the order of 26 kJ (1.5 MJ(mol Pd)$^{-1}$).

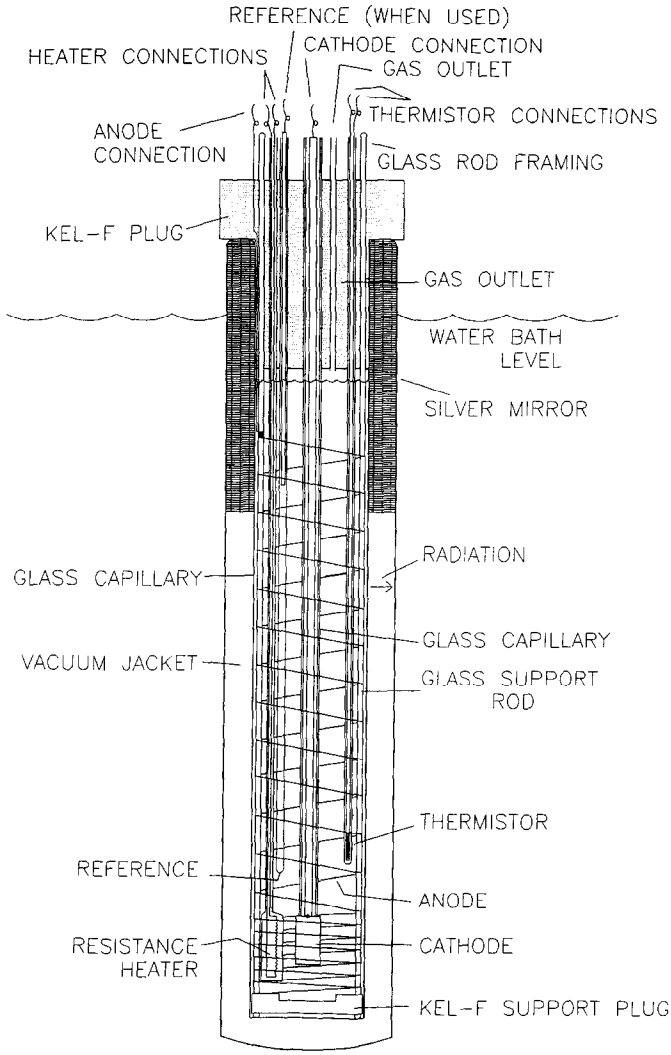

Fig. 2. Schematic diagram of the single compartment vacuum Dewar open calorimeter cells used in this work.

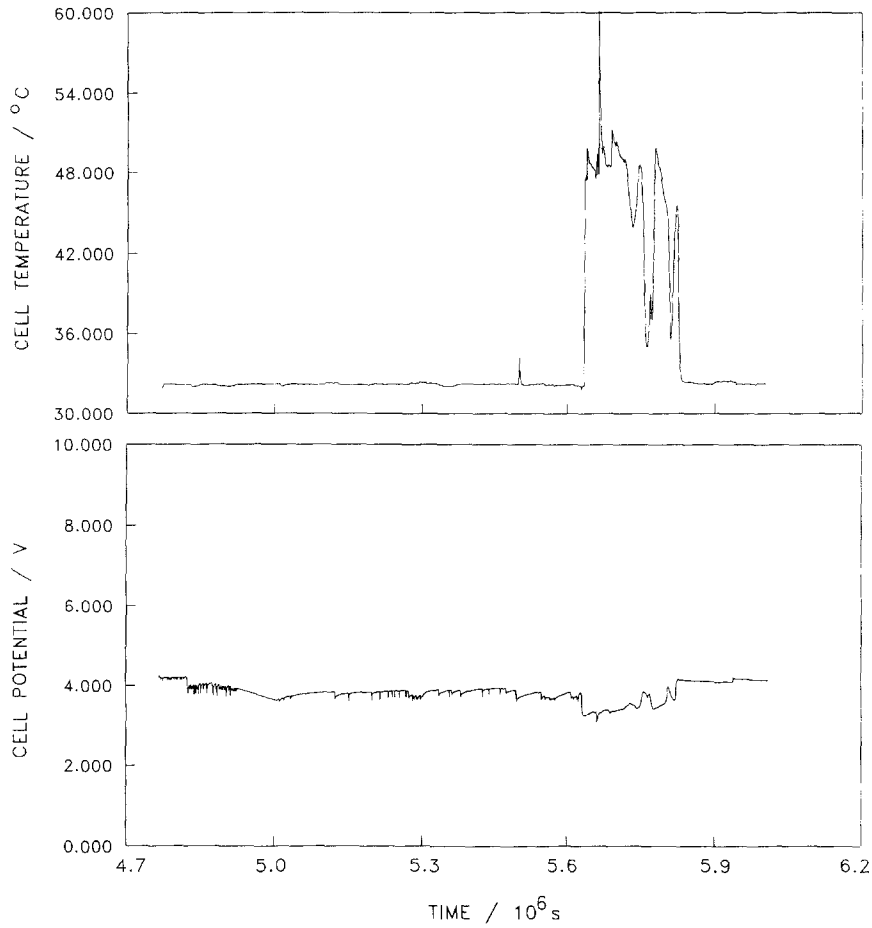

Fig. 3. Cell temperature versus time (upper) and cell potential versus time (lower) plots for a 0.4×1.25 cm Pd rod electrode in 0.1M LiOD solution. Current density 64 mA cm^{-2}, bath temperature 29.87°C.

the rather extreme illustrations of the "bursts" in the rates of excess enthalpy production such as that shown in fig. 3 (for a complete analysis of these "enthalpy bursts" see figs. 8, 9 and 10 of ref. [1]).

At the next level of the quantitative analysis of the experimental data, we naturally require models of the calorimeters and the calibration of the heat transfer to the surrounding water baths. We have shown [1–6] that the behaviour is determined at a close level of approximation by the differential equation

$$C_{P,\mathrm{D_2O},\ell}M^0\frac{\mathrm{d}\Delta\theta}{\mathrm{d}t} = [E_{\mathrm{cell}}(t)-E_{\mathrm{thermoneutral,bath}}]I-\frac{3I}{4F}\frac{P}{P^*-P}[(C_{P,\mathrm{D_2O,g}}-C_{P,\mathrm{D_2O},\ell})\Delta\theta+L]$$

change in the enthalpy content of the calorimeter — enthalpy input due to electrolysis — enthalpy content of the gas stream

$$+\ Q_{\mathrm{f}}(t)\ +\Delta QH(t-t_1)-\Delta QH(t-t_2)-\ k'_{\mathrm{R}}[(\theta_{\mathrm{bath}}+\Delta\theta)^4-\theta^4_{\mathrm{bath}}]\ . \qquad (1)$$

excess enthalpy — heater calibration pulse — radiative heat transfer to the water bath

Here k'_{R} (W K^{-4}) is the heat transfer coefficient which is assumed to be purely radiative: we have shown elsewhere that the neglect of the conductive contribution leads to a small underestimate of $Q_{\mathrm{f}}(t)$. It will be noted

Table 1
Glossary of symbols used and their units.

$C_{P,D_2O,\ell}$	Heat capacity of liquid D_2O, $J\,K^{-1}\,mol^{-1}$
$C_{P,D_2O,g}$	Heat capacity of D_2O vapour, $J\,K^{-1}\,mol^{-1}$
E_{cell}	Measured cell potential, V
$E_{thermoneutral,bath}$	Potential equivalent of the enthalpy of reaction for the dissociation of heavy water at the bath temperature, V
F	Faraday constant, 96484.56 C mol^{-1}
H	Heaviside unity function
I	Cell current, A
k_R^0	Heat transfer coefficient due to radiation at a chosen time origin, $W\,K^{-4}$
(k'_R)	Effective heat transfer coefficient due to radiation, $W\,K^{-4}$
ℓ	Symbol for liquid phase
L	Enthalpy of evaporation, $J\,mol^{-1}$
M^0	Heavy water equivalent of the calorimeter at a chosen time origin, mol
P	Partial pressure, Pa; product species
P^*	Atmospheric pressure, Pa
Q_f	Rate of generation of excess enthalpy, W
$Q_f(t)$	Time-dependent rate of generation of excess enthalpy, W
t	Time, s
ΔQ	Rate of heat dissipation of calibration heater, W
$\Delta\theta$	Difference in cell and bath temperature, K
θ	Absolute temperature, K
θ_{bath}	Bath temperature, K

that one of our preferred methods of calibration uses a "square heating pulse" $\Delta QH(t-t_1)-\Delta QH(t-t_2)$ applied using the resistive heater (fig. 2) (the remaining symbols are defined in table 1).

2. The next level of analysis: the precision and accuracy of the heat transfer coefficients

A very useful next guide to the behaviour of the systems can be obtained by deriving a lower bound of the heat transfer coefficients (designated by $(k'_R)_6$ and/or $(k'_R)_{11}$ in our reports) which is based on the assumption that there is zero excess enthalpy generation within the calorimeters:

$$(k'_R)_{11} = [(\theta_{bath}+\Delta\theta)^4-\theta_{bath}^4]^{-1}\{[E_{cell}(t)-E_{thermoneutral,bath}]I - (3I/4F)[P/(P^*-P)][(C_{P,D_2O,g}-C_{P,D_2O,\ell})\Delta\theta+L]-C_{P,D_2O,\ell}M^0\,d\Delta\theta/dt\}\,. \quad (2)$$

The reason why $(k'_R)_{11}$ is a lower bound is because the inclusion of any process leading to the generation of heat within the cells (specifically the absorption of D (or H) within the lattice or the generation of excess enthalpy within the electrodes) would increase the derived value of this coefficient: $(k'_R)_{11}$ will be equal to the true value of the heat transfer coefficient only if there is no such source of excess enthalpy in the cells as would be expected to hold, for example, for the polarisation of Pt in D_2O solutions (fig. 4). The simplest procedure is to evaluate these coefficients at a set of fixed times following the addition of D_2O to make up for losses due to electrolysis and/or evaporation. Convenient positions are just before the times, t_1, at which the calibrating heating pulses are applied to the resistive heaters (fig. 5). For the particular experiment illustrated in fig. 4, the mean value of 19 such measurements is 0.7280×10^{-9} $W\,K^{-4}$ with a standard deviation $\sigma_{(k'_R)_{11}}=0.0013\times10^{-9}$ $W\,K^{-4}$ or 0.17% of the mean.

It is evident therefore that even such simple procedures can give precise values of the heat transfer coefficients but, needless to say, it is also necessary to determine their accuracy. We have always done this at the next level of complication by applying the heater pulses $\Delta QH(t-t_1)-\Delta QH(t-t_2)$ and by making a thermal

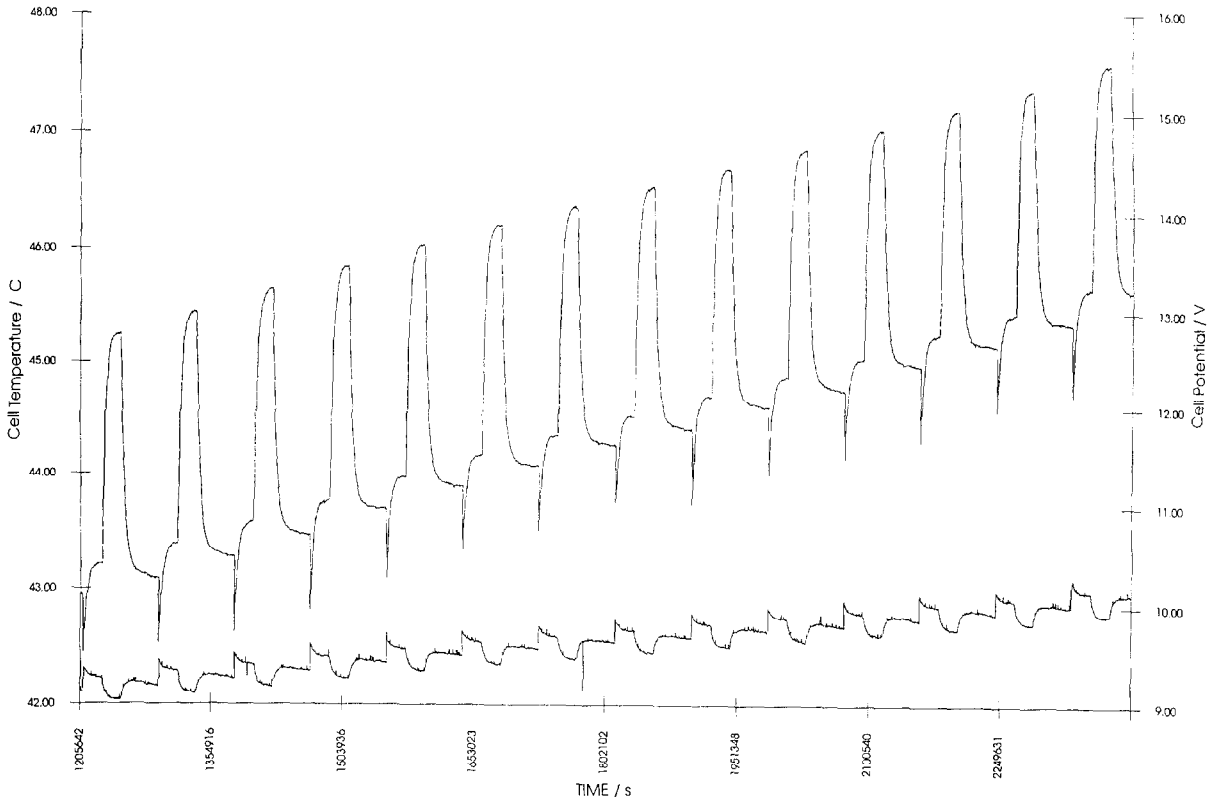

Fig. 4. Segment of a temperature–time/cell potential–time response (with 0.250 W heat calibration pulses) for a cell containing a 12.5×1.5 mm platinum electrode polarised in 0.1M LiOD at 0.250 A.

balance just before the termination of this pulse at $t=t_2$. This time is chosen so that

$$t_2 - t_1 \geqslant 6\tau\,, \tag{3}$$

where τ is the thermal relaxation time

$$\tau \simeq \frac{M^0 C_{P,\mathrm{D_2O},\ell}}{4k'_{\mathrm{R}}\,\theta^3_{\mathrm{bath}}}\,. \tag{4}$$

The scheme of calculation is illustrated in fig. 5: we determine the temperatures and cell potentials at t_2 as well as the interpolated values $(\Delta\theta_1, t_2)$ and $[E_{\mathrm{cell}}(\Delta\theta_1), t_2]$ which would apply in the absence of the heater calibration pulse. We derive the heat transfer coefficient which we have designated as $(k'_{\mathrm{R}})_2$ using

$$\begin{aligned}(k'_{\mathrm{R}})_2 = {} & [(\theta_{\mathrm{bath}}+\Delta\theta_2)^4-(\theta_{\mathrm{bath}}+\Delta\theta_1)^4]^{-1}(\Delta Q-\{[E_{\mathrm{cell}}(\Delta\theta_1), t_2]-[E_{\mathrm{cell}}(\Delta\theta_2), t_2]\}I \\ & -(3I/4F)\{[P_2/(P^*-P_2)][(C_{P,\mathrm{D_2O,g}}-C_{P,\mathrm{D_2O},\ell})\Delta\theta_2+L] \\ & -[P_1/(P^*-P_1)][(C_{P,\mathrm{D_2O,g}}-C_{P,\mathrm{D_2O},\ell})\Delta\theta_1+L]\})\,.\end{aligned} \tag{5}$$

The mean value of $(k'_{\mathrm{R}})_2$ for the particular example of the set of 19 measurements for Pt polarised in D_2O is 0.7264 $\mathrm{W\,K^{-4}}$ with a standard deviation $\sigma_{(k'_{\mathrm{R}})_2}=0.0099\ \mathrm{W\,K^{-4}}$ or 1.4% of the mean.

We make the following additional observations about the calibration of these cells:

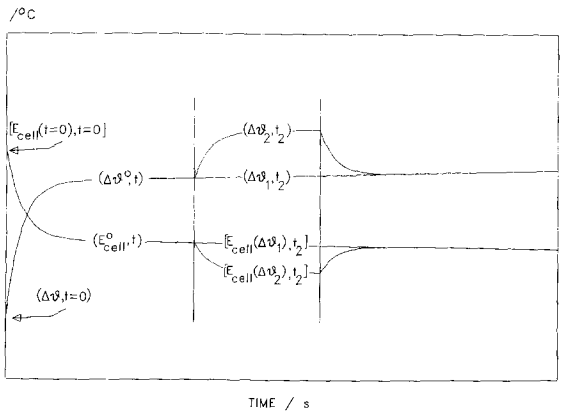

Fig. 5. Schematic diagram of the methodology used for the calculations.

(i) The value of $(k'_R)_{11}$ is close to that given by the product of the Boltzmann coefficient and the radiant surface area.

(ii) $(k'_R)_{11}$ is accurate as well as precise if there are no sources of excess enthalpy in the cells.

(iii) As expected, the precision of $(k'_R)_2$ is lower than that of $(k'_R)_{11}$ (due to division by the differences of two comparably large quantities $((\theta_{bath}+\Delta\theta_2)^4-(\theta_{bath}+\Delta\theta_1)^4)$ rather than by $(\theta_{bath}+\Delta\theta)^4-\theta^4_{bath}$).

(iv) The lowering of the precision of $(k'_R)_2$ can be avoided by using non-linear regression procedures to fit the whole of the $\Delta\theta$–t transient to the model of the calorimeter or by applying low pass filtering (such as the Kalman filter [8,9]) to sections of the time series. The values of the heat transfer coefficients derived (designated by $(k'_R)_5$ in our reports) agree closely with those of $(k'_R)_{11}$ if $Q_f(t)=0$ and we conclude that $(k'_R)_{11}$ is accurate as well as precise under these conditions. We will not discuss $(k'_R)_2$ and $(k'_R)_5$ further in this paper (related simplified methods of data analysis will be described elsewhere [9]). Instead, we outline one of the major objectives of our preliminary investigations which has been to determine what information can be derived for the Pd–H_2O and Pd–D_2O systems using $(k'_R)_{11}$ evaluated point-by-point and bearing in mind the precision and accuracy of blank experiments using Pt cathodes.

(v) We do, however, draw attention once again to the fact that in applying the heat transfer coefficients calibrated with the heater pulse $\Delta QH(t-t_1)-\Delta QH(t-t_2)$ we have frequently used the coefficient defined by

$$(k'_R)_4=[(\theta_{bath}+\Delta\theta_2)^4-(\theta_{bath}+\Delta\theta_1)^4]^{-1}(\Delta Q-(3I/4F)\{[P_2/(P^*-P_2)][(C_{P,D_2O,g}-C_{P,D_2O,\ell})\Delta\theta_2+L]$$
$$-[P_1/(P^*-P_1)][(C_{P,D_2O,g}-C_{P,D_2O,\ell})\Delta\theta_1+L]\}) \quad (6)$$

and determined at $t=t_2$ to make thermal balances at the point just before the application of the calibrating heater pulse (fig. 5). The differences between the use of $(k'_R)_2$ and $(k'_R)_4$ are negligible for blank experiments, which has not been understood by some authors (see, e.g., ref. [10]). However, for the Pd–D_2O and Pd-alloy–D_2O systems the corresponding rates of excess enthalpy generation, $(Q_f)_2$ are significantly larger than $(Q_f)_4$ for fully charged electrodes. The fact that $(Q_f)_2>(Q_f)_4$ as well as other features of the experiments [9] show that there is an element of "positive feedback" between the increase of temperature and the rate of generation of excess enthalpy. The existence of this feedback has been a major factor in the choice of our calorimetric method and especially in the choice of our experimental protocols. As will be shown below, these provide systems which can generate excess enthalpy at specific rates above 1 kW cm^{-3}.

3. Applications of measurements of the lower bound heat transfer coefficients to the investigation of the Pd–D_2O system

In our investigations we have found that a great deal of highly diagnostic qualitative and semi-quantitative

information can be rapidly obtained by examining the time-dependence of $(k'_R)_{11}$. The qualitative information is especially useful in providing an answer to the key question: "Is there excess enthalpy generation within (or at the surface) of Pd-based cathodes polarised in D_2O solutions?"

In order to provide a basis for this investigation, we examine first the time dependence of $(k'_R)_{11}$ in the initial time region for the Pt cathode polarised in D_2O solution (fig. 4). It can be seen from fig. 6 that $(k'_R)_{11}$ rapidly approaches the true steady state value 0.728×10^{-9} W K^{-4}: we conclude that there is no source of excess enthalpy in this system.

For Pd cathodes polarised in H_2O solutions $(k'_R)_{11}$ again approaches the true steady state value with increasing time, e.g., see fig. 7. However, there is now a marked decrease of $(k'_R)_{11}$ at short times. In this case the source of excess enthalpy is due to the heat of absorption of H^+ within the lattice, an effect which decreases with the diffusional relaxation time. The measurement of $(k'_R)_{11}$ in these initial stages is especially sensitive to the presence of such sources because $(\theta_{bath}+\Delta\theta)^4-\theta^4_{bath}\to0$ as $t\to0$ so much so that $(k'_R)_{11}$ is initially negative.

We examine next the results for one Pd cathode polarised in D_2O solutions out of a set of four which will be discussed further in the next section. Figure 8a gives the overall temperature and cell potential–time data for the second electrode of the set. The main objective of these investigations has been to determine the conditions required to produce high rates of excess enthalpy generation at the boiling points of the D_2O solutions. Our protocol for these experiments is based on the hypothesis that the further addition of D^+ to cathodes already highly loaded with deuterium will be endothermic. We therefore charge the electrodes at low to intermediate current densities and temperatures below 50°C for prolonged periods of time; following this, the current densities are increased and the temperature is allowed to rise. The D^+ is then retained in the cathodes and we take advantage of the "positive feedback" to drive the cells to the boiling point (fig. 8).

It can be seen that for these electrodes $(k'_R)_{11}$ is again initially markedly negative due to the dissolution of D^+ in the lattice (fig. 9a). However, in this case $(k'_R)_{11}$ never reaches the true value for this cell, 0.892×10^{-9} W K^{-4} because a second exothermic process develops, namely, the generation of excess enthalpy in the lattice. In view of this, $(k'_R)_{11}$ shows a maximum: these maxima may be strongly or weakly developed depending on the experimental conditions such as the diameters of the electrodes, the current densities, the true heat transfer coefficients, $Q_f(t)$, etc.

We take note here of an important observation: although $(k'_R)_{11}$ never reaches the true value of the heat transfer coefficient, *the maximum values of this lower bound coefficient are the minimum values of* k'_R *which must be used in evaluating the thermal balances for the cells.* The estimates of Q_f derived (which we denote by

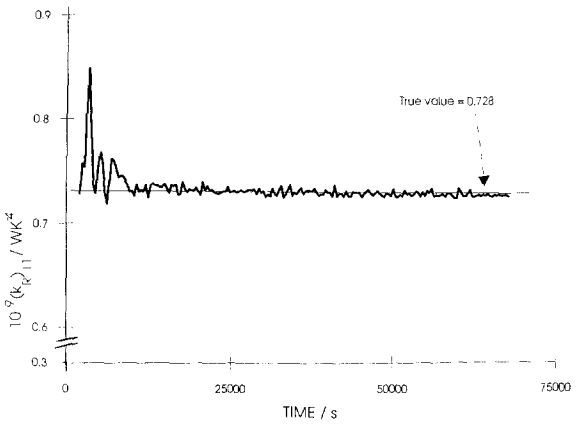

Fig. 6. Plot of the heat transfer coefficient for the first day of electrolysis of the experiment described in fig. 4.

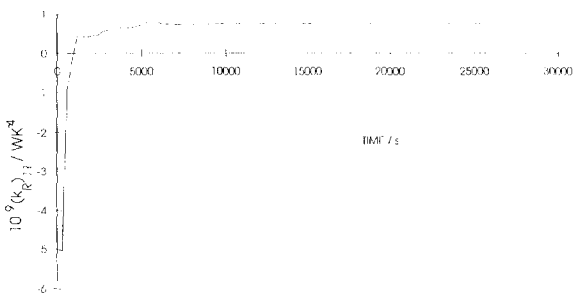

Fig. 7. Plot of the heat transfer coefficient for the first day of electrolysis in a "blank" cell containing a 12.5×2 mm palladium electrode polarised in 0.1M LiOH at 0.250 mA.

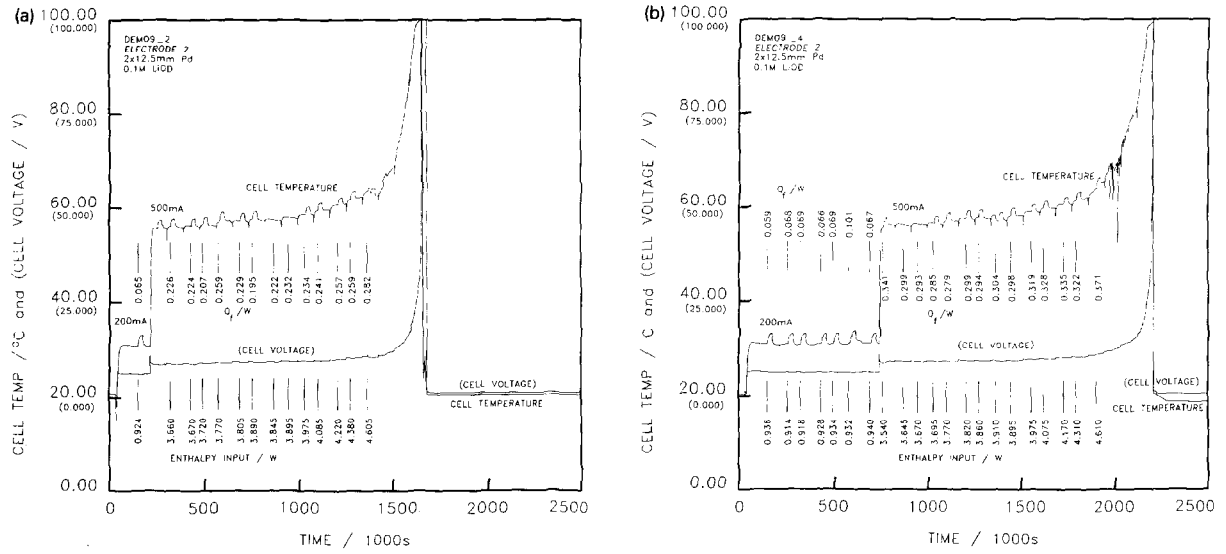

Fig. 8. Temperature–time and potential–time profiles for two of four 12.5×2 mm palladium electrodes polarised in heavy water (0.1M LiOD). Electrolysis was started at the same time for all cells. The input enthalpies and the excess enthalpy outputs at selected times are indicated on the diagrams. The initial current in these cells was 0.200 A, which was increased to 0.500 A at the beginning of days 3 and 9, respectively.

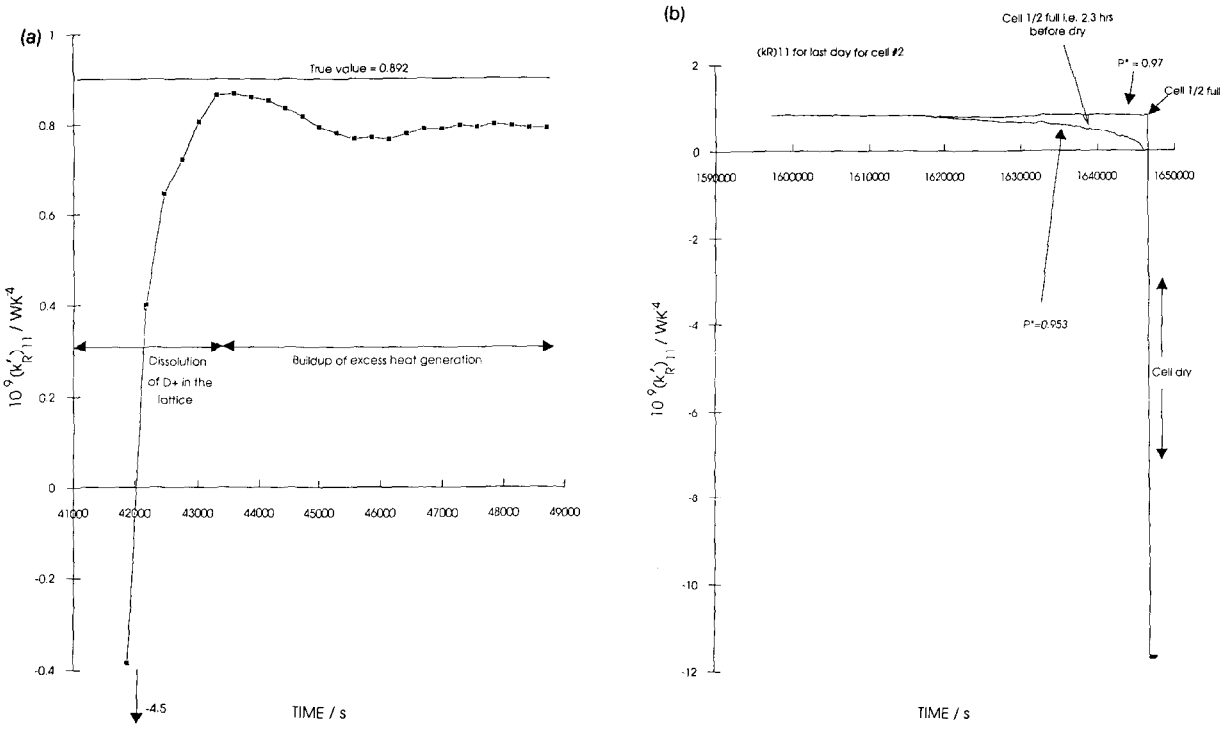

Fig. 9. Plots of the lower bound heat transfer coefficient as a function of time for three different periods of the experiment described in fig. 8a: (a) the first day of electrolysis, (b) the last day of electrolysis.

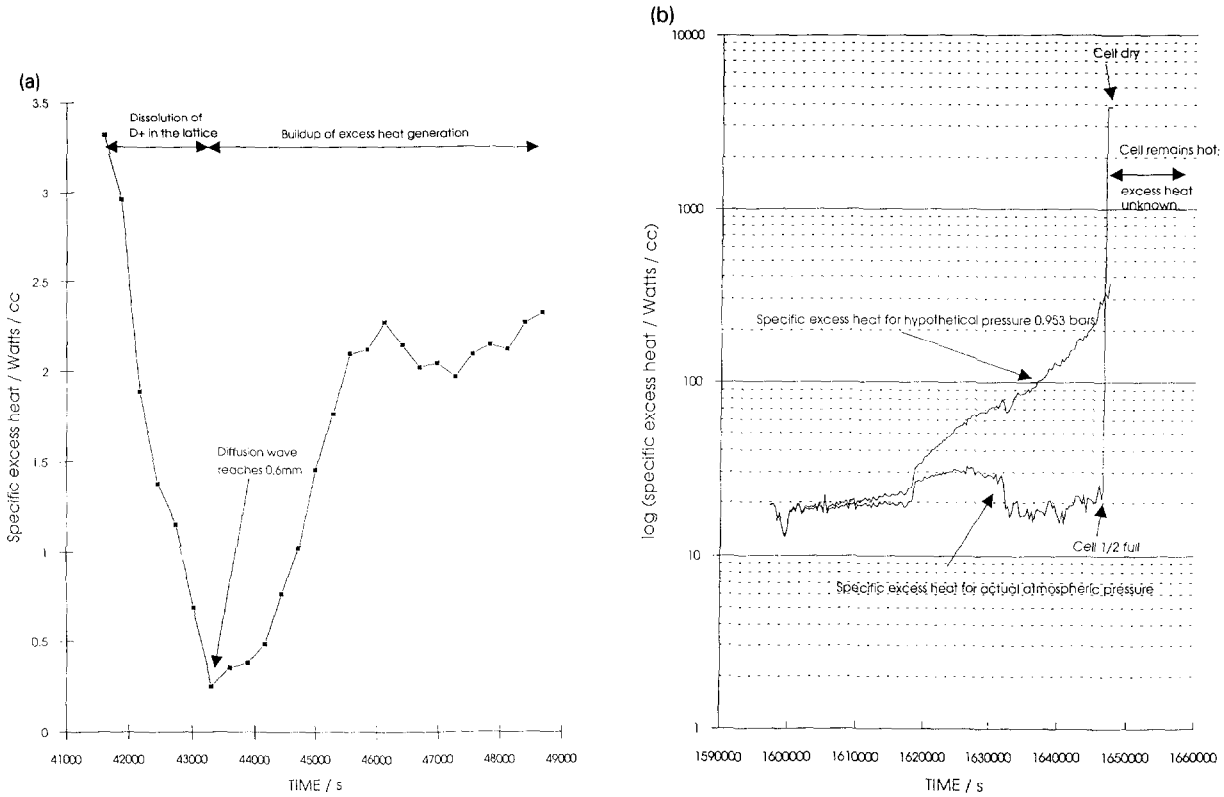

Fig. 10. Plots of the specific excess enthalpy generation for (a) the first and (b) the last day of the experiment described in fig. 8a and using the heat transfer coefficients given in figs. 9a and 9b.

$(Q_f)_{11}$) are in turn lower bounds of the excess enthalpy; fig. 10a gives the values corresponding to the time region covered by fig. 9a. The conclusion that there is excess enthalpy generation is inescapable and we note that this conclusion is independent of any method of calibration which may be adopted to put the study on a quantitative basis. We also note that a similar observation about the significance of our data was made in the independent review which was presented at the Second Annual Conference on Cold Fusion [8].

We discuss here also the last day of operation which is characterised by a rapid rise of temperature up to the boiling point of the electrolyte leading to a short period of intense evaporation (fig. 11 [#1]). The evidence for the time dependence of the cell contents is discussed in the next section. Figure 9b shows the values of $(k'_R)_{11}$ calculated using two assumed atmospheric pressures, 0.953 and 0.97 bar. The first value has been chosen to give a smooth evaporation of the cell contents ($M^0 = 5.0$ D_2O) i.e., no boiling during the period up to the point when the cell becomes dry, 50735 s. However, this particular mode of operation would have required the cell to have been half full at a time 2.3 h before dryness. Furthermore, the ambient pressure at that time was 0.966 bar. We believe therefore that such a mode of operation must be excluded. For the second value of the pressure, 0.97 bar, the cell would have become half empty 11 min before dryness, as observed from the video recordings (see the next section) and this in turn requires a period of intense boiling during the last 11 min. It can be seen that $(k'_R)_{11}$ decreases gradually for the assumed condition $P^* = 0.953$ bar whereas it stays

[#1] In addition to electrolysis, the loss of D_2O from the cells proceeds only by a continuous, smooth flow of vapor through a vent in the top of the cell.

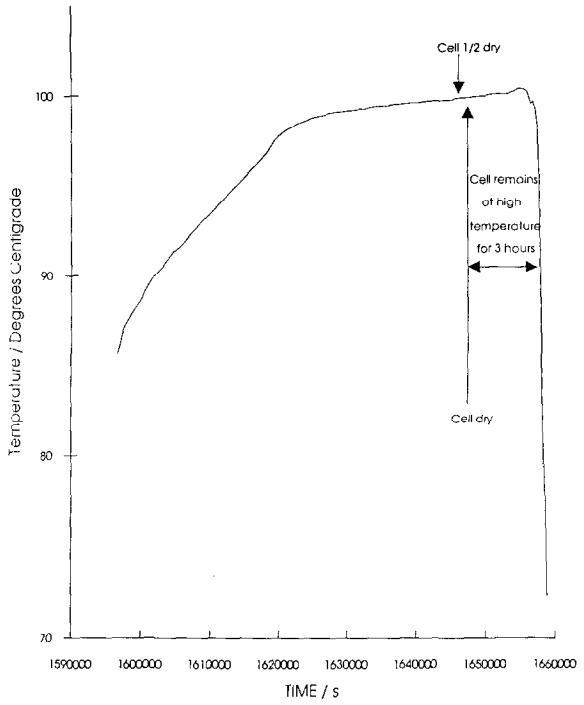

Fig. 11. Expansion of the temperature–time portion of fig. 8a during the final period of rapid boiling and evaporation.

more nearly constant for $P^*=0.97$ bar up to the time at which the cell is half full, followed by a rapid fall to markedly negative values. These markedly negative values naturally are a consequence of the high rates of enthalpy generation required to explain the rapid boiling during the last 11 min of operation. The true behaviour must be close to that calculated for this value of the ambient pressure.

Figure 10b gives the corresponding rates of excess enthalpy generation for these two assumed atmospheric pressures. These rates are initially insensitive to the choice of P^*. However, with increasing time, Q_f for the first condition reaches ~ 300 W cm^{-3} in the final stages. As we have noted above, this particular pattern of operation is not consistent with the ambient atmospheric pressure. The true behaviour must be close to that for $P^*=0.97$ bar for which Q_f remains relatively constant at ~ 20 W cm^{-3} for the bulk of the experiment followed by a rapid rise to ~ 4 kW cm^{-3} as the cell boils dry.

4. A further simple method of investigating the thermal balances for the cells operating in the region of the boiling point

It will be apparent that for cells operating close to the boiling point, the derived values of Q_f and of $(k'_R)_{11}$ become sensitive to the values of the atmospheric pressure (broadly for $\theta_{cell} > 97.5$°C, e.g., see fig. 10b). It is therefore necessary to develop independent means of monitoring the progressive evaporation/boiling of the D_2O. The simplest procedure is to make time-lapse video recordings of the operation of the cells which can be synchronised with the temperature–time and cell potential–time data. Figures 8a and 8b give the records of the operation of two of a set of four such cells. Figure 12, a still taken from the video recordings, shows the last cell being driven to boiling, the first three having boiled dry.

As it is possible to repeatedly reverse and run forward the video recordings at any stage of operation, it also becomes possible to make reasonably accurate estimates of the cell contents. We have chosen to time the evap-

Fig. 12. Still of video recordings of the cells described in fig. 8 showing the last cell during the final boiling period, the other cells having boiled dry.

oration/boiling of the last half of the D_2O in cells of this type and this allows us to make particularly simple thermal balances for the operation in the region of the boiling point. The enthalpy input is estimated from the cell potential–time record, the radiative output is accurately known (temperature measurements become unnecessary!) and the major enthalpy output is due to evaporation of the D_2O. We illustrate this with the behaviour of the cell (figs. 8b, 12).

Calculation. Enthalpy input: By electrolysis, $(E_{cell}-1.54)\times$(cell current) $\simeq 22500$ J.

Enthalpy output: To ambient $\simeq k'_R[(374.5°)^4-(293.15°)^4]\times 600$ s $=6700$ J; in vapour $\simeq$ (2.5 mol $\times$ 41 kJ/mol) $=102500$ J.

Enthalpy balance: Excess enthalpy $\simeq 86700$ J.

Rate of enthalpy input: By electrolysis, 22500 J/600 s $=37.5$ W.

Rate of enthalpy output: To ambient, 6600 J/600 s $=11$ W; in vapour, 102500 J/600 s $\simeq 171$ W.

Balance of enthalpy rates: Excess rate $\simeq 144.5$ W; excess specific rate $\simeq 144.5$ W/0.0392 cm$^3 \simeq 3700$ W cm^{-3}.

We note that the excess rate of energy production is about four times that of the enthalpy input even for this highly inefficient system; the specific excess rates are broadly speaking in line with those achieved in fast breeder reactors. We also draw attention to some further important features: provided satisfactory electrode materials are used, the reproducibility of the experiments is high; following the boiling to dryness and the open-circuiting of the cells, the cells nevertheless remain at high temperature for prolonged periods of time (fig. 11); fur-

thermore the Kel-F supports of the electrodes at the base of the cells melt so that the local temperature must exceed 300°C.

The question of the appropriate materials to use for these experiments remains the most difficult to answer. We can say that across production batches of materials that exhibit excess enthalpy generation, all samples in those batches behave similarly. Samples which exhibit cracking during deuterium loading never exhibit excess enthalpy generation; this problem is prevalent especially in large samples. While we have had some promising samples from various other sources, our highest rates of success have been those obtained from Johnson Matthey, PLC. The interplay of the metallurgical processing procedures, the properties of the materials produced, and the rates of excess enthalpy production (together with the reproducibility of these phenomena) continue to be actively studied.

We conclude once again with some words of warning. A major cause of the rise in cell voltage is undoubtedly the gas volume between the cathode and anode as the temperature approaches the boiling point (i.e., heavy steam). The further development of this work therefore calls for the use of pressurised systems to reduce this gas volume as well as to further raise the operating temperature. Apart from the intrinsic difficulties of operating such systems it is also not at all clear whether the high levels of enthalpy generation achieved in the cells in fig. 12 are in any sense a limit or whether they would not continue to increase with more prolonged operation. At a specific excess rate of enthalpy production of 2 kW cm^{-3}, the electrodes in the cells of fig. 12 are already at the limit at which there would be a switch from nucleate to film boiling if the current flow were interrupted (we have shown in separate experiments that heat transfer rates in the range 1–10 kW cm^{-2} can be achieved provided current flow is maintained i.e., this current flow extends the nucleate boiling regime). The possible consequences of a switch to film boiling are not clear at this stage. We have therefore chosen to work with "open" systems and to allow the cells to boil to dryness before interrupting the current.

References

[1] M. Fleischmann, S. Pons, M.W. Anderson, L.J. Li and M. Hawkins, J. Electroanal. Chem. 287 (1990) 293.
[2] M. Fleischmann and S. Pons, Fusion Technol. 17 (1990) 669.
[3] S. Pons and M. Fleischmann, in: Proc. First Annual Conf. on Cold Fusion, Salt Lake City, UT, 28–31 March 1990.
[4] S. Pons and M. Fleischmann, in: The science of cold fusion: Proc. Second Annual Conf. on Cold Fusion, Como, Italy, 29 June–4 July 1991, eds. T. Bressani, E. del Guidice and G. Preparata, Vol. 33 of the Conference Proceedings of The Italian Physical Society (Bologna, 1992) p. 349.
[5] M. Fleischmann and S. Pons, J. Electroanal. Chem. 332 (1992) 33.
[6] M. Fleischmann and S. Pons, Proc. Third Annual Conf. on Cold Fusion, ICCF3, Nagoya, Japan, 21–25 October 1992, submitted.
[7] M. Fleischmann, in: The science of cold fusion: Proc. Second Annual Conf. on Cold Fusion, Como, Italy, 29 June–4 July 1991, eds. T. Bressani, E. del Guidice and G. Preparata, Vol. 33 of the Conference Proceedings of The Italian Physical Society (Bologna, 1992) p. 475.
[8] W. Hansen, Report to the Utah State Fusion Energy Council on the Analysis of Selected Pons–Fleischmann Calorimetric Data, in: The science of cold fusion: Proc. Second Annual Conf. on Cold Fusion, Como, Italy, 29 June–4 July 1991, eds. T. Bressani, E. del Guidice and G. Preparata, Vol. 33 of the Conference Proceedings of The Italian Physical Society (Bologna, 1992) p. 491.
[9] S. Pons and M. Fleischmann, to be published.
[10] R.H. Wilson, J.W. Bray, P.G. Kosky, H.B. Vakil and F.G. Will, J. Electroanal. Chem. 332 (1992) 1.